Artifacts in cranial MRI caused by extracranial foreign bodies and analysis of these foreign bodies

Selim Kayaci, Ahmet Tabak[1], Irmak Durur-Subasi[2], Tugba Eldes[3], Vaner Koksal[4], Murat Sirin[5], Yusuf Kemal Arslan[6]

Departments of Neurosurgery and [6]Biostatistics, Faculty of Medicine, Erzincan University, Erzincan, [1]Department of Chemistry, Faculty of Arts and Sciences, Sinop University, Departments of [3]Radiology and [4]Neurosurgery, Faculty of Medicine, Recep Tayyip Erdogan University, [5]Department of Physics, Faculty of Arts and Sciences, Recep Tayyip Erdogan University, Rize, [2]Department of Radiology, Dışkapı Training and Research Hospital, Ankara, Turkey

Correspondence: Dr. Selim Kayacı, Department of Neurosurgery, Faculty of Medicine, Erzincan University, Rize, Turkey.
E-mail: selim_kayacı@hotmail.com

Abstract

Purpose: The purpose of our study was to conduct a chemical analysis of extracranial foreign bodies (FBs) causing artifacts in cranial magnetic resonance imaging (MRI) and to investigate the association between chemical composition, magnetic susceptibility, and artifact size. **Materials and Methods:** A total of 12 patients were included in the study. The FBs responsible for the artifacts were visualized using cranial computed tomography (CT). Artifact-causing FBs were removed from the scalps of 10 patients and analyzed using scanning electron microscope with energy dispersive spectroscopy (SEM-EDS), X-ray diffraction spectroscopy (X-RD), and Fourier-transform infrared spectroscopy (FT-IR). The magnetic susceptibility of the samples was determined using the reference standard material $MnCl_2.6H_2O$. The volume of the MRI artifacts was measured in cubic centimeters (cm^3). **Results:** EDS results demonstrated that the mean Fe ratio was 5.82% in the stone samples and 0.08% in the glass samples. Although no phase peaks were detected in the X-RD spectra of the glass samples, peaks of Fe_2O_3, Al_2Ca (SiO_4) were detected in the X-RD spectra of the stone samples. The FT-IR spectra revealed metal oxide peaks corresponding to Fe, Al, in the stone samples and peaks confirming Al_2SiO_5 and Na_2SiO_3 structures in the glass samples. The mean volumes of the MRI artifacts produced by the stone and glass samples were 5.9 cm^3 and 2.5 cm^3, respectively. **Conclusions:** Artifacts caused by extracranial FBs containing metal/metal oxide components are directly associated with their chemical composition and the artifact size are also related to element composition and magnetic susceptibility.

Key words: Artifact; glass; magnetism; magnetic resonance imaging; stone

Introduction

Although magnetic resonance imaging (MRI) is a safe and effective diagnostic tool, artifacts caused by certain foreign bodies (FBs) found in the body are a misleading problem. An artifact is defined as a deviation of the visual integrity of an anatomic structure. Substantial artifacts may appear due to patient movements, blood flow through large vessels, and metallic clips implanted during surgery.[1] Metallic artifacts often appear as a field of low signal intensity surrounded by a high-intensity signal. The image spectrum may appear as

Access this article online	
Quick Response Code:	Website: www.ijri.org
	DOI: 10.4103/ijri.IJRI_211_18

Cite this article as: Kayaci S, Tabak A, Durur-Subasi I, Eldes T, Koksal V, Sirin M, *et al*. Artifacts in cranial MRI caused by extracranial foreign bodies and analysis of these foreign bodies. Indian J Radiol Imaging 2019;29:299-304.

Received: 22-May-2018 **Revision:** 02-Dec-2018
Accepted: 03-Sep-2019 **Published:** 30-Oct-2019

spatial distortion, an isolated low-density area, or multiple high-density rings.[2] Magnetic FBs (substances which interact with magnetic fields) are classified into three groups according to their magnetic susceptibility: ferromagnetic with dependent magnetic permeability (DMP) much greater than 1 (DMP>>>1); paramagnetic, with DMP slightly greater than 1 (DMP >1); and diamagnetic, with DMP slightly less than 1 (DMP <1).

Ferromagnetic bodies such as Fe, Mg, Co, Ni, and Cr_2O_3 are strongly affected and become magnetized in magnetic fields. Paramagnetic bodies such as Al, Pt, Li, Ta, and Mo may be slightly magnetized in a magnetic field and slightly increase the strength of a magnetic field. Diamagnetic bodies such as wood, Zn, Cu, Ag, Bi, and Au have a very weak effect on magnetic fields.[3] Thus, diamagnetic bodies have low risk for artifact formation in MRI, whereas ferromagnetic and paramagnetic bodies have a high potential for artifact formation in MRI.[4]

Artifacts in cranial MRI may be caused by metallic neurosurgical implants, dental implants, cosmetic products such as hair dye and concealers, coloring agents, and particles of metal drill tips used during surgery. However, there are no previous studies of artifact-inducing millimetric stone and glass bodies in the scalp. In the present study, we used cranial CT to visualize magnetic metal-containing FBs such as stone and glass samples in the scalp that caused MRI artifacts, then we removed the FBs and analyzed their chemical composition. In summary, we investigated the association between the chemical composition of these samples and the apparent size of the artifacts they produced on cranial MRI.

Materials and Methods

Patient population and radiological examination

The study included 12 patients who presented with neurologic symptoms such as headache and dizziness to the Neurology and Neurosurgery outpatient clinic of Medical Faculty Training Hospital between December 2011 and January 2016 and exhibited artifacts on cranial MRI. This is a prospective study and the patients have been randomly selected. The study was approved by the Institutional Ethics Committee, and informed consent was taken from all the patients. MRI examinations were performed in a 1.5-T scanner (Gyroscan Intera; Philips Medical Systems, Best, Netherlands). Standard precautions were taken to ensure patient safety during the MRI procedure. It was not possible to identify the body causing these artifacts by MRI. Therefore, cranial CT was done in all patients to examine for FBs causing the artifacts (16-slice, Philips MX 16, Philips Medical Systems, Best, Netherlands). In 10 of these 12 patients, the FBs responsible for the artifacts were detected using cranial CT. In the other 2 patients, who had both undergone burr-hole craniostomy due to chronic subdural hematoma, no artifact-causing FBs were detected on cranial CT.

Chemical and physical processes

In the 10 patients, FBs were detected on CT. These were removed through a 2-4 cm incision in the scalp due to scarring from previous head trauma. The FBs measurements are taken from the CT as two largest dimensions. Then half of the average of two size (width and length) are used as the radius for a spherical shape. The volume of the foreign material is calculated as in $4/3\ \pi r^3$ formula.[5]

Composition analyses of the excised FBs were conducted using SEM-EDS, X-RD, and FT-IR. The samples were dried for approximately 12 h at 105°C in a drying oven to remove absorbed water and humidity from the surfaces and pores of the materials. SEM and SEM-EDS analyses of the glass and stone samples were performed using the Jeol/JSM-6610 (Tokyo, Japan) and Oxford Instruments Inca X-Act/51-ADD0013 (Abingdon, Oxfordshire, UK) devices. X-RD spectra of the samples were obtained using the X-ray diffraction technique in Rigaku/Smart Lab (Tokyo, Japan) diffractometer (= 1,54050 Å wavelength Cu K/40 kV/40 mA). FT-IR spectra of all samples were recorded in the 4,000-200 cm-1 range using a Spectrum 100 (Perkin Elmer, Ohio, USA) spectrophotometer. In addition, the magnetic susceptibility of samples was determined by magnetic susceptibility balance (Sherwood Scientific Ltd, Cambridge, UK) using the reference standard material $MnCl_2.6H_2O$.

Calculation of the artifact volume according to the Cavalieri Principle

In 10 patients, the volume of the MRI artifact was calculated in cm^3. The artifact volume were used to calculate volumes using Cavalieri principle and planimetry technique. Surface area of the artifact on MR images converted to DICOM format in volume calculations were calculated by planimetry method using Image J analysis program. Each measurement was performed blindly by the same person at least three times in the program, and the mean value was recorded. The artifact volume was calculated by summarizing the sum of surface areas in the following formula, as described previously.[6]

$$V = t \times \sum A$$

In the above equation, t denotes the thickness of the consecutive sections and ΣA denotes the total surface area of the thimble in the section view. All data were entered into a Microsoft Excel spreads heet which automatically calculated the values based on the above formula. Theeach cranium MRI artifact volume was calculated separately.

Statistical analyses

The results were presented for continuous variables as mean ± standard deviation, median (min-max), and for categorical variables as *n* (%). Due to the sample size ($n = 5$ in each group) comparisons between groups were done using Mann-Whitney U test. The relation between magnetic sensibility and artifact volume was analyzed with the

Spearman rank correlation coefficients and results were presented as r (p). A *P* value <0.05 was considered to be statistically significant. Statistical analysis was performed using the IBM SPSS version 19 package programme (IBM Software, New York, United States).

Results

Radiological findings

MRI artifacts appeared as bone and parenchymal signal loss. The cranial CT scans of 10 of these patients revealed artifact-causing FBs. Figure 1A-C shows FB images from patients in whom cranial CT revealed stone or glass samples responsible for the artifacts seen in cranial MRI, as well as from patients exhibiting MRI artifacts after burr-hole craniostomy. In Figure 2, calculation of artifact volume is shown as an example. Mean volume of the MRI artifacts created by the 5 stone samples were 5.9 cm^3 (range, 3.6-9.2 cm^3) and that of the artifacts caused by the 5 glass samples were 2.5 cm^3 (range, 1.8-3.2 cm^3). Mean volume of the stone samples were 0.155 cm^3 (range, 0.078-0.299 cm^3) and that mean volume of the glass samples were 0.223 cm^3 (range, 0.097-0.357 cm^3) [Table 1].

Chemical and physical findings

SEM images of the stone and glass samples revealed that stone had a crystalline and irregularly layered complex structure, while glass had a relatively amorphous structure [Figure 3]. The results of EDS analysis showed that the samples included various metal/metal oxide components [Table 2]. The mean Fe and Si ratios were 5.82% (range, 0.5-13.7%) and 19.4% (range, 4.8-44.6%) in the stone samples, and 0.08% (range, 0.0-0.2%) and 29.66% (range, 29.9-44.6%) in the glass samples, respectively. While no phase peaks were detected in X-RD spectra of the glass samples due to their amorphous structure, the X-RD spectra of the stone samples revealed peaks at approximately 24.42 (2q) and 50.14 (2q) degrees for Fe_2O_3; at 22.02 (2q) and 27.84 (2q) degrees for Al_2Ca (SiO_4); at 26.67 (2q) and 39.56 (2q) degrees for SiO_2; and 25.70 (2q) degrees for TiO_2 [Figure 4].

FT-IR spectrum evaluation of the samples revealed water O-H stretch and bend peaks at approximately 3,400 cm^{-1} and 1,620 cm^{-1}, respectively, C-H stretch peaks at 2,923 cm^{-1} from organic content, Si-O-Si stretch peaks at 1,096 and 1,032 cm^{-1}, and CO_3 stretch peaks from calcite at 1,425 cm^{-1} [Figure 5]. In addition, metal oxide (M-O) peaks in the 600-400 cm^{-1} range in the stone samples indicated the presence of Fe, Al, Mg, and TiO_2, and peaks in the 1,100-400 cm^{-1} range clearly confirmed the presence of Al_2SiO_5 and Na_2SiO_3 structures [Figure 5].

The mean magnetic susceptibility values of the samples were 2,742 (range, 440-5,980) for glass samples and >10,000 (range, 9,260->10,000) for stone samples. There was a positive correlation (r = 0.92; P < 0.001) between magnetic susceptibility and artifact volume [Table 1].

Table 1: Magnetic susceptibility, artifact volume values and volume of the foreign bodies

Case no-sample	Magnetic susceptibility	Artifact volumes (cm^3)	Volume of the foreign bodies (cm^3)
1-Stone	9260	3.6	0.078
2-Stone	>10000	4.2	0.087
3-Stone	>10000	9.2	0.147
4-Stone	>10000	4.8	0.164
5-Stone	>10000	7.8	0.299
Mean	>10000	5.9	0.155
6-Glass	720	1.8	0.357
7-Glass	5980	2.4	0.097
8-Glass	440	2.2	0.164
9-Glass	5680	3.2	0.268
10-Glass	890	3.0	0.230
Mean	2742	2.5 cm3	0.223

It shows that positive relationship between magnetic susceptibility and artifact volume (r=0.92; P<0.001)

Table 2: Element composition determined by EDS

	Element composition and ratios (%)										
Case no-sample	Fe	Al	Si	Mg	Na	Ti	Mn	K	Ca	O	Other elements
1-Stone	0.5	1.2	41.5	0	0.7	0	0	0	0.3	55.8	0
2-Stone	1.4	0.3	0.9	7.6	0	0	0	0	23.3	52.5	13.0
3-Stone	13.7	8.2	15.8	6.9	0	0.2	0.2	1.2	1.2	52.5	0.3
4-Stone	2.2	9.3	25	0.5	1.0	0.3	0	1.7	4.6	55.4	0.1
5-Stone	11.3	7.1	12.2	6.2	0	1.4	0.3	0.1	4.2	55.8	0.2
Mean	5.82	5.22	19.4	4.31	0.34	0.38	0.25	0.6	6.72	54.4	2.7
6-Glass	0	1.5	44.6	0	2.7	0	0	0.9	0.1	50.2	1.0
7-Glass	0.2	0	29.6	0	13.5	0	0	0	4.2	52.5	0
8-Glass	0	1.5	42.4	0	3.3	0	0	0	0	50.9	1.9
9-Glass	0.2	3.8	4.8	1.1	0.3	0	0	0	15.4	50.2	24.8
10-Glass	0	0.6	29.9	2.6	10.1	0	0	0	5.3	51.5	0.6
Mean	0.08	1.48	29.6	0.74	5.98	0	0	0	5.0	51.2	5.6

For all stone samples, the standard deviation (SD) of Fe was±0.2. In one of the stone samples, the SD of Ca was±0.2. In three of the glass samples, the SD of Si was±0.2. For all other elements in other samples, the SD was ±0.1

Discussion

Teitelbaum *et al*. stated that a mild artifact is smaller than the body that causes it, a moderate artifact is approximately the same size as the body that causes it, and a severe black hole artifact is larger than the body causing it.[7] Somasundaram and Kalavathi investigated the types and causes of artifacts in cranial MRI and showed that artifacts caused by ferromagnetic/paramagnetic implants have the appearance of craniectomy defect and tissue defect (pronounced gap) in brain parenchyma.[8] In our study, the artifacts were larger than the stone and glass bodies producing them. And the artifacts caused by stone and glass bodies were physically and geometrically similar to the images obtained by Somasundaram and Kalavathi.

It has been shown that there are several factors that affect the size of the artifact in MRI[9-16]: type and thickness of

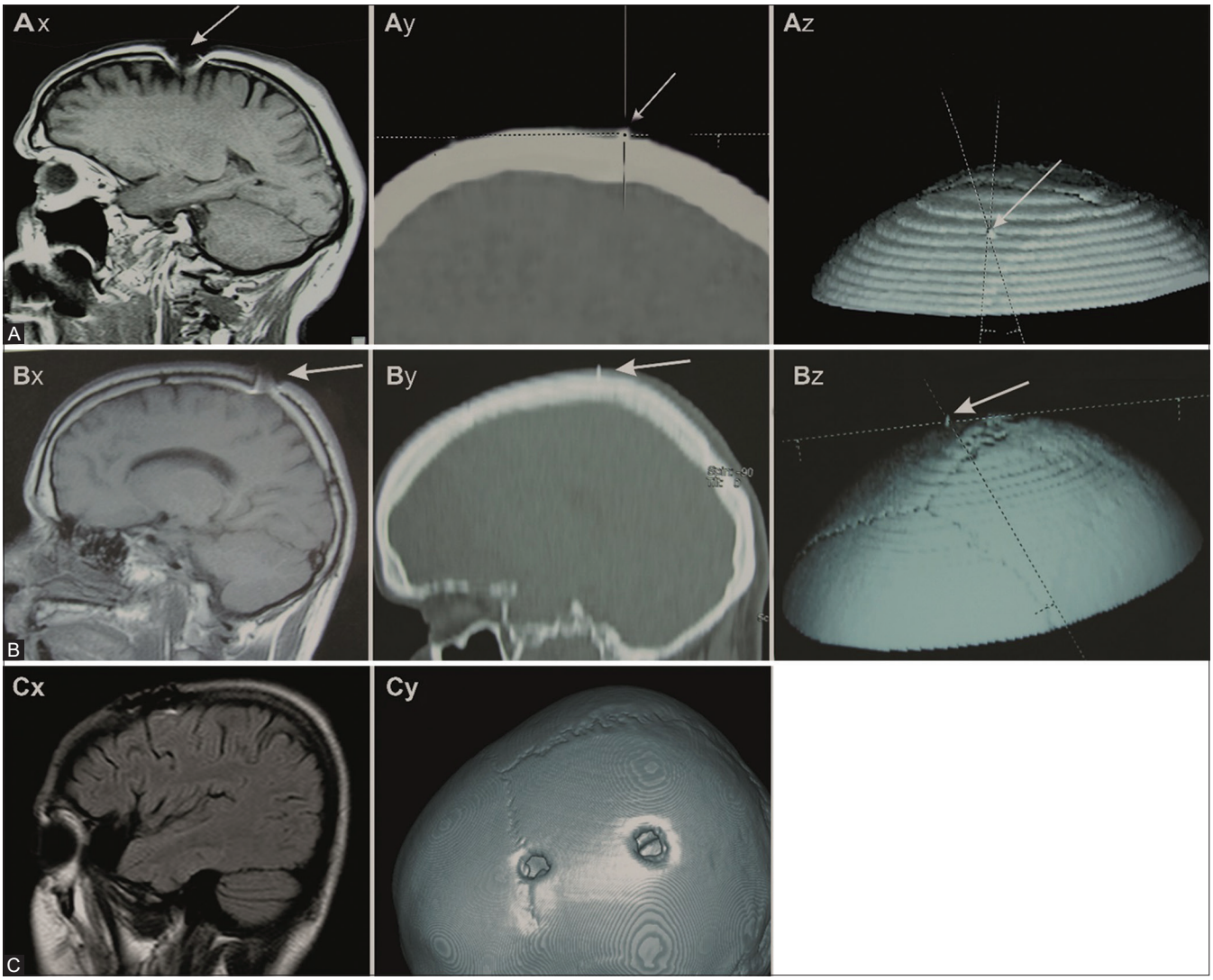

Figure 1 (A-C): Example radiological images from selected patients. (A) Foreign body in the scalp after a traffic accident (stone sample). Ax. MRI artifact in the parietal aspect of the sagittal plane; Ay. Cranial CT reveals material 5.1 × 5 mm in the right parietal aspect of the sagittal plane; Az. 3D cranial CT image of the same patient. (B) Foreign body in the scalp due to head trauma (glass sample). Bx. Artifact in the parietal aspect of the sagittal plane of cranial MRI; By. Glass particle measuring 15 × 2.6 mm in left parietal aspect of the coronal plane on cranial CT; Bz. 3D cranial CT image of the same patient. (C) Patient who underwent surgery due to chronic subdural hematoma. Cx. Cranial MRI in postoperative month 2 showing signal distortion appearing as bone loss in the left frontal burr-hole region; Cy. No foreign body that could cause an artifact in the burr hole region was detected in 3D cranial CT

magnetic object used, shape and orientation of the object, radiofrequency and receiver bandwidths and the static field strength. Unlike the aforementioned studies, in the present study we investigated the relationship between MRI artifact volume and the chemical content of the FBs. Our findings demonstrate that stone samples containing higher levels of elements such as Fe, Mg, and Ti highly affected the magnetic field and therefore created larger artifacts. However, we found that glass samples containing higher levels of elements such as Si and Na had lesser effect on the magnetic field. Therefore, the artifacts formed by glass samples were smaller than those due to stone particles.

Even when no metallic bodies are used during cranial surgery, artifacts may still appear on MRI. These artifacts may be to result from metal particles introduced by metal drill tips. These tiny metallic FBs may not be detected in direct radiography or cranial CT.[17] Heindel *et al*. reported that artifacts were caused by bone fragments created during trepanation.[18] They attributed this phenomenon to the amalgamation of bone fragments and minute metal particles from surgical instruments. A study involving the imaging of Fe powder in water demonstrated that microscopic levels (even as low as 0.01 mg) of ferromagnetic FBs could cause artifacts in MRI.[19] Two patients in the present series had a history of cranial surgery. These patients underwent burr-hole craniostomy with closed-system drainage due to chronic subdural hematoma. No neurosurgical implants that can cause artifacts were used during the surgery.

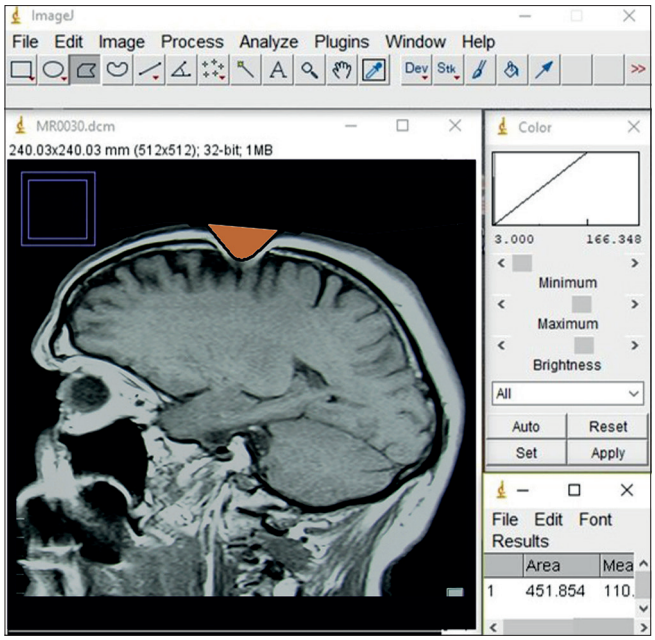

Figure 2: Calculation of surface area of the artifact volume with Image J analysis program

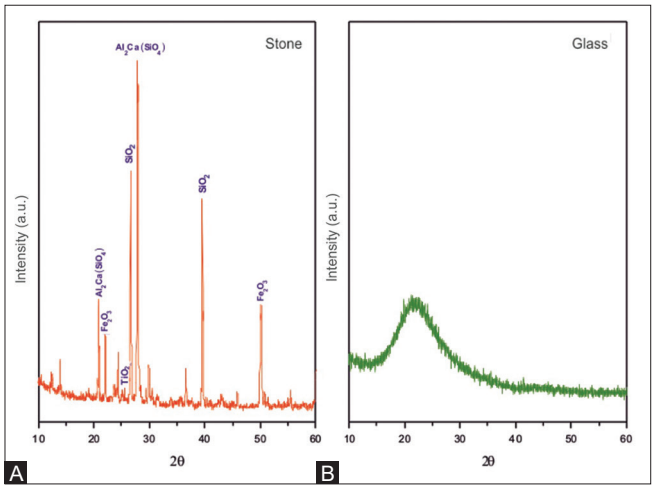

Figure 4 (A and B): X-RD values of the stone (A) and glass (B) samples. The X-RD spectra of the stone samples revealed peaks of Fe_2O_3 at approximately 24.42 (2q) and 50.14 (2q) degrees, of Al_2Ca (SiO_4) at 22.02 (2q) and 27.84 (2q) degrees, of SiO_2 at 26.67 (2q) and 39.56 (2q) degrees, and of TiO_2 at 25.70 (2q) degrees. The X-RD spectra of the glass samples revealed no phase peaks

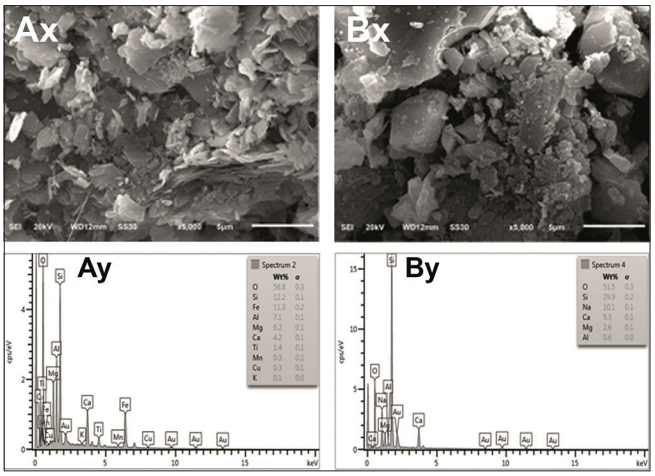

Figure 3 (A and B): SEM and EDS images of the glass (A) and stone (B) samples. Ax. SEM image of stone sample; Ay. EDS results of stone sample. Bx. SEM image of glass sample; By. EDS results of glass sample

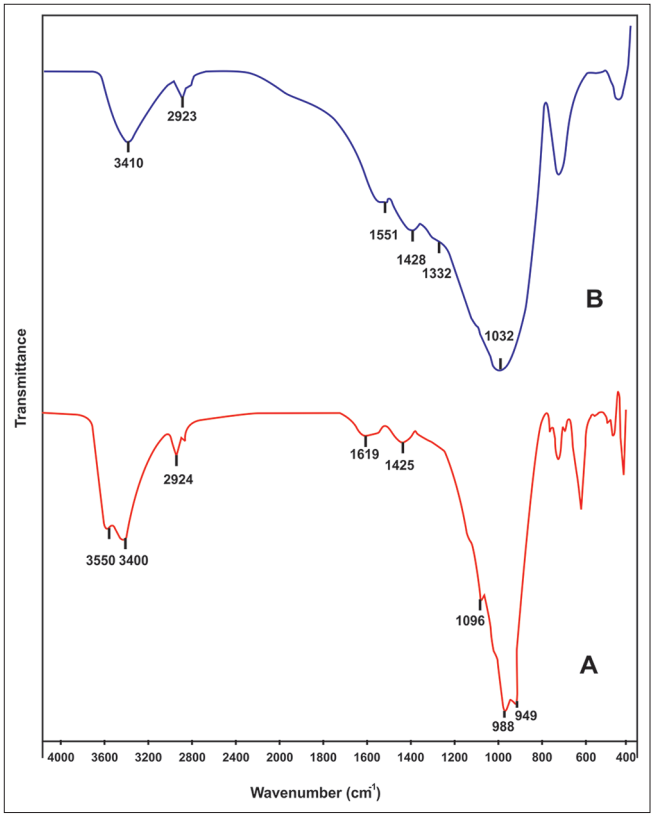

Figure 5 (A and B): FT-IR spectra of the stone (A) and glass (B) samples. The peaks detected in the glass samples in the 1100-400 cm^{-1} range indicate the presence of Al_2Ca (SiO_4) and Na_2SiO_3, and metal oxide (M-O) peaks in the 600-400 cm^{-1} range demonstrate Fe, Al, Mg, and TiO_2 content

According to the EDS analysis results obtained from this study, the elemental composition of the stone and glass samples were different. We determined that the Fe ratio in stone samples were 72.7 times higher than in glass samples. Likewise, stone samples contained 5.8 times more Mg and 3.5 times more Al than glass samples. Three of the stone samples had at low K content. However, K was detected in trace amounts in only one of the glass samples. Mn was detected in only one stone sample and none of the glass samples. In three of the stone samples, there were a low level of Ti, but no Ti was detected in the glass samples. The glass samples had 17.5 times higher Na ratio and 1.5 times higher Si ratio than that of stone samples. The glass and stone samples contained comparable amounts of Ca.

As noted above, stone samples contain ferromagnetic elements such as Fe, Mg, Ti more than glass samples. Therefore, they affected the magnetic field more strongly. It is conceivable that the magnetic properties of the glass

samples may also be related to the presence of various metal/metal oxide components within the Al_2SiO_5 network and to the structural characteristics of glass. Glass is generally alkali-silicate based and may include metal oxides compatible with this network structure.[20,21] Analysis of our EDS results also showed the presence of metal components such as Na_2O-SiO_2, Na_2O, Al_2O_3, and SiO_2 in the glass samples. In this study, we determined that glass samples contained higher proportions of paramagnetic elements such as Al and Si, and therefore interacted less with the magnetic field compared to stone sapmles.

Previous studies have shown that stone and glass bodies contain elements that affect the magnetic field and give them magnetic susceptibility.[22,23] Our X-RD, FT-IR spectra results clearly indicated this. In this study, we found that the magnetic susceptibility of stone is approximately 5 times higher than that of glass. This result supports the previous data and interpretations of spectroscopic measurements of stone and glass samples.[24,25] We also determined that artifacts created by stone have approximately twice the volume of those formed by glass.

Conclusion

Our results indicate that artifact volume is directly associated with chemical composition and magnetic susceptibility. The stone samples had higher Fe, Mg, and Ti content and also caused much larger artifacts on MRI compared to the glass samples. Similarly, the magnetic susceptibility of stone samples was higher than that of glass.

Declaration of patient consent

The authors certify that they have obtained all appropriate patient consent forms. In the form the patient(s) has/have given his/her/their consent for his/her/their images and other clinical information to be reported in the journal. The patients understand that their names and initials will not be published and due efforts will be made to conceal their identity, but anonymity cannot be guaranteed.

Financial support and sponsorship

Nil.

Conflicts of interest

There are no conflicts of interest.

References

1. Joseph PM, Atlas SW. Artifacts in MR. In: Atlas SW, editor. Magnetic Resonance İmaging of the Brain and Spine. 3rd ed. Philadelphia: Lippincott, Williams, Wilkins; 2002. p. 239-75.
2. Pusey E, Lufkin RB, Brown RK, Solomon MA, Stark DD, Tarr RW, *et al*. WN. Magnetic resonance imaging artifacts: Mechanism and clinical significance. RadioGraphics 1986;6:891-911.
3. Mathew CA, Maller S, Waran M. Interactions between magnetic resonance imaging and dental material. J Pharm Bioallied Sci 2013;5:113-6.
4. Shafiei F, Honda E, Takahashi H, Sasaki T. Artifacts from dental casting alloys in magnetic resonance imaging. J Dent Res 2003;82:602-6.
5. Lakits A, Prokesch R, Scholda C, Bankier A, Weninger F, Imhof H. Multiplanar imaging in the preoperative assessment of metallic intraocular foreign bodies. Helical computed tomography versus conventional computed tomography. Ophthalmology 1998;105:1679-85.
6. Acer N, Sahin B, Bas O, Ertekin T, Usanmaz M. Comparison of three methods for the estimation of total intracranial volume: Stereologic, planimetric, and anthropometric approaches. Ann Plast Surg 2007; 58:48-53.
7. Teitelbaum GP, Bradley WG Jr, Klein BD. MR ımaging artifacts, ferromagnetism, and magnetic torque of ıntravascular filters, stents, and coils. Radiology 1988;166:657-64.
8. Somasundaram K, Kalavathi P. Analysis of ımaging artifacts in MR brain ımages. Oriental J Computer Sci Technol 2012; 5:135-41.
9. Bartels LW, Smits HFM, Bakker CJG, Viergever MA. MR imaging of vascular stents: Effects of susceptibility, flow, and radiofrequency eddy currents. JVIR 2001;12: 365-71.
10. Bennett LH, Wang PS, Donahue MJ. Artifacts in magnetic resonance imaging from metals. J Appl Phys 1996;79: 4712-4.
11. Camacho CR, Plewes DB, Henkelman RM. Nonsusceptibility artifacts due to metallic objects in MR imaging. J Magn Reson Imag 1995; 5:75-88.
12. Ganapathi M, Joseph G, Savage R, Jones AR, Timms B, Lyons K. MRI susceptibility artefacts related to scaphoid screws: The effect of screw type, screw orientation and imaging parameters. J Hand Surg (British and European Volume) 2002; 27:165-70.
13. Olsen RV, Munk PL, Lee MJ, Janzen DL, Mackay AL, Xiang QS, *et al*. Metal artifact reduction sequence: Early clinical applications. Radiographics 2000; 20:699-712.
14. Cho ZH, Kim DJ, Kim YK. Total inhomogeneity correction including chemical shifts and susceptibility by view angle tilting. Med Phys 1988; 15:7-11.
15. Czerny C, Krestan C, Imhof H, Trattnig S. Magnetic resonance imaging of the postoperative hip. Top Magn Reson Imaging 1999; 10:214-20.
16. Suh JS, Jeong EK, Shin KH, Cho JH, Na JB, Kim DH, *et al*. Minimizing artifacts caused by metallic implants at MR imaging: Experimental and clinical studies. AJR Am J Roentgenol 1998;171:1207-13.
17. Tetsumura A, Honda E, Sasaki T, Kino K. Metallic residues as a source of artifacts in magnetic resonance imaging of the temporomandibular joint. Dentomaxillofac Radiol 1999;28:186-90.
18. Heindel W, Friedmann G, Bunke J, Thomas R, Firsching R, Ernestus RI. Artifacts in MR imaging after surgical intervention. J Comput Assist Tomogr 1996;10:596-9.
19. Alanen A, Bondestam S, Kome M. Artifacts in MR imaging caused by small quantities of powdered iron. Acta Radiol 1995;36:92-5.
20. Mekki A, Khattak GD, Holland D, Chinkhota M, Wenger LE. Structure and magnetic properties of vanadium–sodium silicate glasses. J Non Cryst Solids 2003;318:193-201.
21. Mazurin OV. Glass properties: Compilation, evaluation, and prediction. J Non Cryst Solids 2005;351:1103-12.
22. Moosbrugger C. ASM Ready Reference: Electrical and Magnetic Properties of Metals, ASM International, Materials Park, OH 44073-0002, Printed in the United States of America; 2000.
23. Wijn HPJ, editor. Magnetic Properties of Metals, d-Elements, Alloys and Compounds. Springer-Verlag Berlin Heidelberg; 1991. p. 1-21.
24. Theil Kuhn L, A Bojesen, Timmermann L, Meedom Nielsen M, Morup S. Structural and magnetic properties of core–shell iron–iron oxide nanoparticles. J Phys Condens Mat 2002;14:49.
25. Shokrollahi H, Janghorban K. Soft magnetic composite materials (SMCs). J Mater Process Technol 2007;189:1-12.